Decoding tissue-specific TGF-β signaling in pulmonary arterial hypertension: from genetic predisposition to mechanobiology

Becher, C.

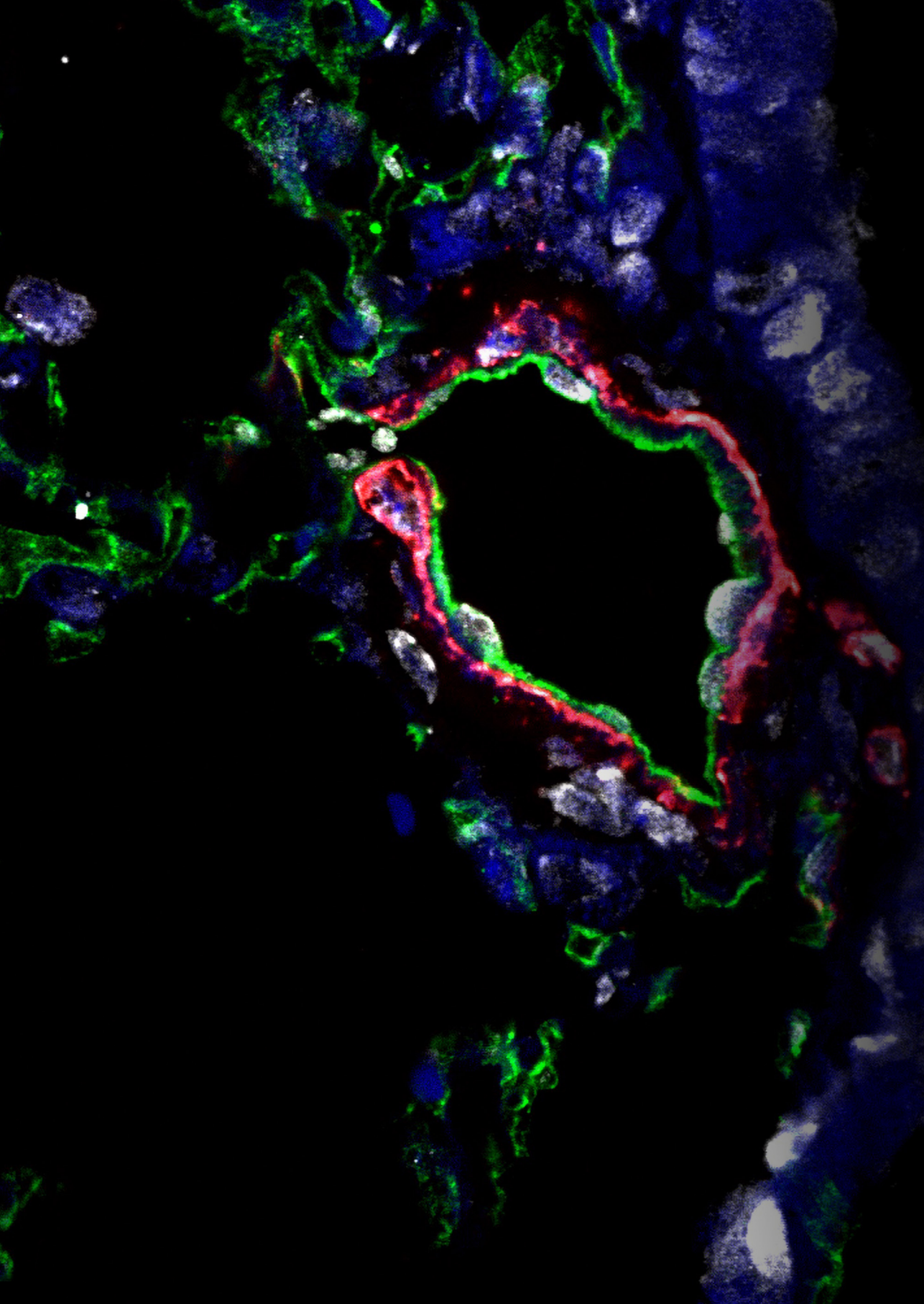

Part 2

3

BMP9 Modulates IL-33 Signaling to Mitigate EndMT in Pulmonary Arterial Hypertension

Regulation of EndMT in PAH by BMP9 and IL-33

Clarissa Becher, Esmee J Groeneveld, Rozenn Quarck, Beau Neep, Pan Xiaoke, Robert Szulcek, Ly Tu, Christophe Guignabert, Harm Jan Bogaard, Paul B Yu, Frances de Man, Gonzalo Sanchez-Duffhues, Marie-José Goumans

Hypertension. 2026 Feb;83(2):e24916. doi: 10.1161/HYPERTENSIONAHA.125.24916.

Abstract

Background

Pulmonary Arterial Hypertension (PAH) is a progressive disorder involving disrupted Bone Morphogenetic Protein (BMP) signaling, pulmonary inflammation, and endothelial-to-mesenchymal transition (EndMT). We hypothesized that IL-33 signaling contributes to PAH progression by inducing EndMT and interacting with BMP9, a key modulator of inflammation and vascular remodeling.

Methods

IL-33 expression was assessed in lung tissues from Sugen/hypoxia and control mice, as well as in pulmonary arterial endothelial cells (PAECs) and lung tissues from patients with PAH and healthy donors. EndMT and signaling pathways were analyzed in PAECs and microvascular endothelial cells (MVECs) exposed to IL-33, BMP9, and sST2 (soluble suppression of tumorigenicity 2) using quantitative polymerase chain reaction, Western blotting, ELISA, and immunostaining. Plasma BMP9 and sST2 levels were quantified in patients with PAH..

Results

Immunofluorescent analysis revealed elevated IL-33 expression in pulmonary endothelial cells of SuHx mice compared to controls, consistent with findings in PAECs from PAH patients. BMP9 significantly upregulated sST2 expression in human PAEC and MVECs, inhibited IL-33 target gene expression, and effectively suppressed IL-33-induced EndMT. Notably, BMP9 demonstrated greater efficacy in preventing EndMT compared to recombinant soluble ST2 or ST2L-neutralizing antibodies. Circulating BMP9 and sST2 levels in PAH patient plasma were positively correlated in specific patient groups stratified by sex, age, and NYHA functional class, suggesting a protective role of BMP9 in modulating IL-33-induced EndMT.

Conclusions

BMP9 plays a protective role against IL-33-induced EndMT in PAECs by upregulating sST2 expression and neutralizing IL-33, suggesting that targeting the IL-33 signaling pathway may represent a promising therapeutic strategy to mitigate EndMT in PAH.

Key words

Bone morphogenetic protein, endothelial dysfunction, Transforming Growth Factor-β, pulmonary endothelial cells.

Non-standard Abbreviations and Acronyms

BMP, bone morphogenetic protein; EndMT, endothelial-to-mesenchymal transition; MVEC; microvascular endothelial cells; PAEC, pulmonary arterial endothelial cells.

Graphical Abstract

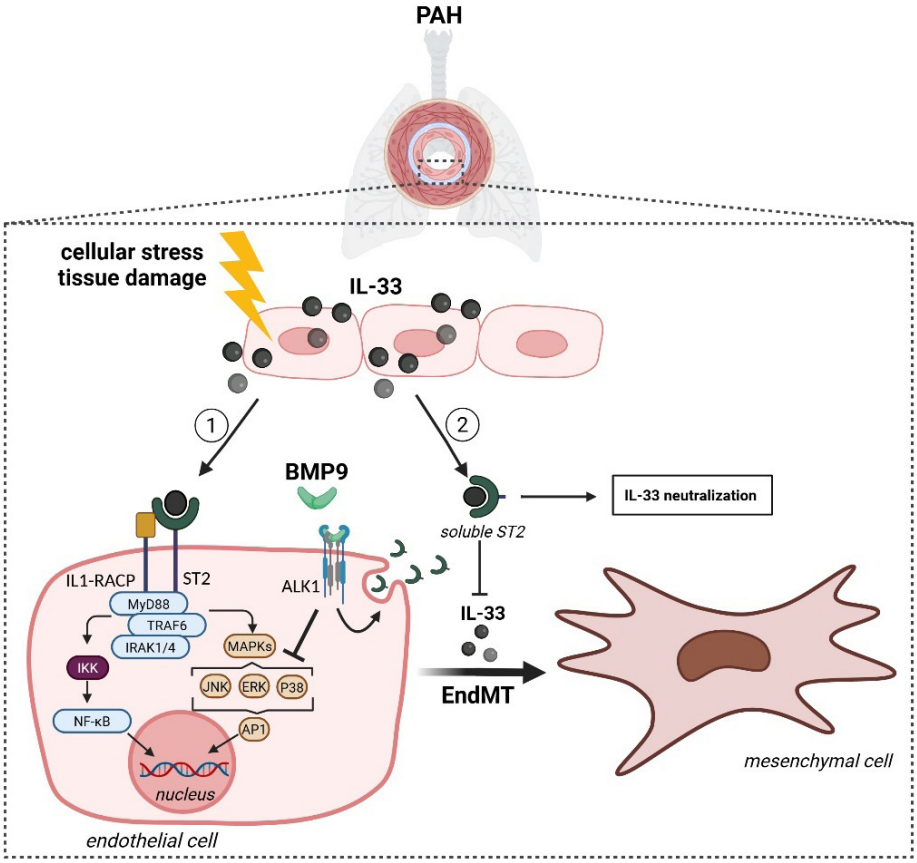

Introduction

Pulmonary arterial hypertension (PAH) is a severe and rare disorder defined as elevated pulmonary arterial pressure (>20 mmHg) and pulmonary vascular resistance (>2 Wood Units). PAH is characterized by progressive occlusive remodelling of the distal pulmonary vasculature, resulting in increased pulmonary artery pressure, right ventricular (RV) dysfunction, RV failure, and death if left untreated[1]. Key pathological processes include the dysregulated proliferation of endothelial cells (EC) and smooth muscle cells (SMC), inflammation, apoptosis, and thrombosis. Structural abnormalities in the pulmonary arteries, such as medial and intimal thickening, capillary rarefaction, and the formation of disorganized plexiform lesions, are hallmarks of PAH[2]. The defining feature of these changes is the elevated presence of cells expressing α-smooth muscle actin (α-SMA), indicative of a transition of ECs into mesenchymal-like cells, contributing to vascular remodelling. This process, known as endothelial-to-mesenchymal transition (EndMT), is characterized by the loss of endothelial markers, such as CD31 and vascular endothelial (VE)-cadherin, with simultaneous acquisition of mesenchymal markers including α-SMA, transgelin (SM22α), fibronectin, and vimentin. EndMT disrupts vascular barrier function, cell-cell adhesion, cell migration, and immune cell infiltration, thereby playing a pivotal role in the vascular remodelling associated with PAH[3]. Mutations in the Bone Morphogenetic Protein Receptor Type 2 (*BMPR2*) gene are frequently implicated in PAH pathogenesis. Combined with inflammatory signals, these mutations are thought to suppress BMPR2 expression while exacerbating pathological Transforming Growth Factor (TGF-β) signaling[4]. In PAH patients, circulating TGF-β1 and activin A levels are elevated[5,6]. This imbalance has prompted the exploration of therapeutic strategies targeting the TGF-β pathway, such as sotatercept — a GDF and activin ligand trap (ACVRIIA-Fc) recently approved by the FDA as a first-in-class add-on treatment for adults with PAH — and approaches aimed at enhancing BMP9 activity, have been explored[7]. However, the role of BMP9 in PAH remains controversial. While some studies suggest that enhancing BMP9 is beneficial, others report that genetic deletion or inhibition of BMP9 mitigates the onset and progression of PAH[8]. Despite these conflicting findings, BMP9 is recognized to be crucial for cardiovascular homeostasis and implicated in PH development, with its role appearing context- and time-dependent, particularly in pulmonary endothelium. Congruently, previous research indicates that the impact of BMP9 in the vasculature is strongly influenced by inflammatory responses[9]. Interleukin-33 (IL-33), part of the IL-1 cytokine family, is produced by barrier cells like epithelial and ECs during cellular stress

or tissue injury and functions as an alarmin[10]. IL-33 signals through its unique receptor ST2, forming a complex with IL-1 receptor accessory protein (IL-1RAcP or IL1RAP). This signaling cascade activates pathways such as mitogen-activated protein kinases (MAPKs) and nuclear factor- κB (NF-κB) mediated by the adaptor protein myeloid differentiation primary response protein 88 (MyD88)[11]. The soluble form of ST2 (sST2) functions as a decoy receptor, effectively neutralizing IL-33 activity. Aberrant IL-33 signaling has been implicated in various lung diseases, including chronic obstructive pulmonary disease (COPD), asthma, and allergic and airway inflammatory disorders[12]. In a murine model of hypoxia-induced PH, IL-33 has been shown to exacerbate vascular remodelling under hypoxic conditions[13]. In addition, IL-33 signaling stimulates the proliferation of control PAEC, while blockade of the membrane-bound ST2 receptor (ST2L) reduces these effects in a Sugen/Hypoxia (SuHx) mouse model[14].

We hypothesized that altered pulmonary vascular IL-33 expression would perpetuate PAH progression through the induction of EndMT and interaction with the BMP9 signaling pathway. Using primary PAECs and MVECs from PAH patients, experimental animal models, and patient cohorts, we unveil a new crosstalk between IL-33 and BMP9 in the regulation of EndMT in PAH. Specifically, BMP9 was shown to inhibit EndMT in pulmonary ECs by upregulating sST2. In patient cohorts, we observed elevated sST2 levels in males, individuals over 67 years of age, and more severe PAH patients. A positive correlation was observed between sST2 and BMP9 levels within these stratified groups, highlighting their potential interplay in PAH pathogenesis.

Materials and Methods

Reagents

Human recombinant BMP4 (#314-BP-010/CF), BMP6 (#507-BP-020/CF), BMP9 (#3209-BP-010/CF), BMP10 (#2926-BP-025/CF), Activin A (#338-AC-010/CF), TGFb1 (#240-B-010/CF), and recombinant human soluble ST2/IL-33R Fc (#523-ST-100), were obtained from R&D Systems. Human recombinant Interleukin-33 (IL-33) (#CYT-425) was purchased from Prospec, and LDN-193189 (#6053), a selective BMP signaling inhibitor targeting Alk1/2/3 and six other kinases, was purchased from Tocris (supplemental material table 1). Carrier-free ligands were reconstituted in 4 mM HCl, 0.1% BSA.

Blood samples

Patients diagnosed with idiopathic PAH and hereditary PAH, according to the European Respiratory Society (ERS) and European Society of Cardiology (ESC) guidelines, who underwent right heart catheterization for diagnosis purposes at the University Hospital Leuven (Belgium) between 2009 and December 2023, were included[1]. Blood samples were collected on ethylenediaminetetra-acetic acid at the time of diagnostic right heart catheterization, and plasma was prepared as previously described[15]. The study protocol was approved by the Institutional Ethics Committee of the University Hospital Leuven, and all participants gave written informed consent.

Cell culture

PAEC and MVEC were isolated from healthy controls or patients with PAH. PAH cells were obtained from lung tissue during transplantation, while control cells were derived from noncancerous lung tissue dissected from pneumonectomy patients. Patient characteristics of the cells are displayed in Table S2. The study was approved by the VU University Medical Center ethics board (protocol-nr: 2012/306, non-WMO [Wet Medisch-wetenschappelijk Onderzoek met mensen]) and performed as previously described.16 Both cell types were cultured on 0.1% (w/v) gelatin-coated (Sigma-Aldrich, G1890) culture ware (Corning) in complete EC medium (ScienCell, 1001) supplemented with 100-U/mL Pen/Strep, 1% EC growth supplement, and 5% FCS. Cells were maintained at 37°C and 5% CO_2 in a humidified atmosphere and regularly tested for mycoplasma.

EndMT assay

PAECs from patients with PAH or healthy donors were cultured in Lan-Tek II chamber slides (Thermo Fisher, 154534) with ECM complete medium. At 80% confluence, cells were treated with BMP9 (1 ng/mL, 3 hours), rsST2 (recombinant soluble ST2; 1 µg/mL), ST2 neutralizing antibody (1 µg/mL), or vehicle control (30 minutes), followed by IL-33 (100 ng/mL, 72 hours). Subsequent fixation, immunostaining, and image acquisition were performed, as described in the Supplemental Methods. Negative control stainings were performed, and representative images are provided in Figure S6 to confirm antibody specificity.

siRNA Experiments

PAECs were transfected with 25-nM ON-TARGETplus SMARTpool siRNAs targeting ALK1 (L-005302-02-0005, Dharmacon), ENG (endoglin; L-011026-00-0005, Dharmacon), or nontargeting control siRNA (siScr, D-001810-10-20;

Dharmacon) using the manufacturer's protocol in antibiotic-free medium. After 24 hours, the medium was replaced with standard culture medium containing FCS and penicillin/streptomycin for an additional 24 hours. Cells were then starved overnight and stimulated with BMP9 (1 ng/mL) for 3 hours before RNA isolation for quantitative polymerase chain reaction analysis.

Reverse transcription-quantitative PCR (RT-qPCR)

Cells were cultured in 12-well plates with ECM complete medium until 80% confluence and then starved (6 hours) in ECM basal medium with 0.1% FBS. Cells were incubated (16 hours) with TGF-β1 (1 ng/mL), activin A (50 ng/mL), or vehicle control. Alternatively, they were treated (3 hours) with BMP4, BMP6 (50 ng/mL each), BMP9, BMP10 (1 ng/mL each), or ligand buffer. The different stimulation times reflect the faster signaling kinetics of BMPs compared with the slower response of TGF-β ligands in ECs. For inhibition assays, cells were pretreated (30 minutes) with LDN-193189 (120 nmol/L) or dimethyl sulfoxide, followed by BMP9 (1 ng/mL, 3 hours). RNA was extracted using the RNA Miniprep System (Promega, Z6012) after PBS washes. cDNA synthesis was performed with 500-ng RNA using the RevertAid First Strand cDNA Synthesis Kit (Thermo Fisher, K1632). Reverse transcription-quantitative polymerase chain reaction was conducted with GoTaq SYBR Green Supermix (Promega, A6001) on a CFX384 Connect Real-Time PCR System (Bio-Rad) per manufacturer's protocol. Ct values were normalized to Glyceraldehyde-3-phosphate dehydrogenase) GAPDH and Actin Related Protien (ARP) using the ΔΔCt method. Primer sequences and specificities are listed in Table S4. To distinguish between the isoforms of Interleukin-1 Recpetor-Like 1 (IL1RL1), isoform-specific primers were designed. For sST2, the forward primer was placed within the unique exon 1, corresponding to transcript NM_003856.4, ensuring specificity for the soluble isoform. For ST2L, transcript NM_016232.5 served as the reference, and primers were selected from regions absent in the sST2 transcript. Primer specificity was verified using NCBI Primer-BLAST against the respective transcript FASTA sequences.

Western Blotting

Cells were cultured in 12-well plates with ECM complete medium until confluence and then starved (6 hours) in ECM basal medium with 0.1% FBS. Cells were stimulated with BMP9 (1 ng/mL) or ligand buffer (16 hours). Where indicated, cells were pretreated with rsST2 (1 μg/mL, 30 minutes) before IL-33 (100 ng/mL) stimulation for 5, 15, or 60 minutes. Lysates were subsequently obtained and processed as indicated in the Supplemental Material. All original blots are provided in the Supplemental Material.

Enzyme-linked immunosorbent assay (ELISA)

Cells were cultured in 24-well plates with ECM complete medium until 80% confluency, and then starved for 16h. After pre-incubation with BMP9 (1 ng/mL, 3h), IL-33 (100 ng/mL) or vehicle control was added for 24h. Supernatants were collected, centrifuged (1000×g, 20 min, 4˚C), and used for protein detection assays. Cytokine and sST2 levels were measured using human IL-33 DuoSET ELISA (R&D Systems, #DY3625B) and human sST2 ELISA (Elabscience, #E-EL-H6082) per manufacturer's instructions. sST2 and BMP9 levels in PAH patient plasma were quantified using ELISA kits from Elabscience (#E-EL-H6082) and R&D Systems (#DY3209), respectively.

Immunohistochemical staining

Mouse lung slices were prepared as described previously.17 Briefly, 6-month-old male C57 Black 6J mice received weekly subcutaneous SU-5416 (20-mg/kg) injections and were placed in 10% O_2 hypoxia for 3 weeks; a separate cohort remained in normoxia. Human lung tissues were obtained postautopsy from patients with PAH and control subjects without cardiopulmonary abnormalities. Immunohistochemical staining and image analysis of lung sections were performed, as detailed in the Supplemental Methods. Representative images of negative control stainings were performed to confirm antibody specificity (Figure S6).

Statistical analysis

Each cell culture experiment was independently replicated at least three times. Statistical analyses and graphing were performed using GraphPad Prism v9 (GraphPad Software). Data were analyzed using Student's t-tests or one-/two-way ANOVAs with Tukey post-hoc tests for multiple comparisons, as detailed in figure legends. Normality was assessed using the Shapiro-Wilk test. Non-normally distributed values were log-transformed and expressed as medians with 95% confidence intervals. If log-transformed data were normally distributed, comparisons were made using parametric t-tests; otherwise, the Mann-Whitney test was used. Pearson and Spearman correlations were applied to normally and non-normally distributed variables, respectively. A p-value < 0.05 was considered statistically significant.

Results

IL-33 expression is increased in human PAEC from PAH patients and in pulmonary vessels of Sugen/Hypoxia mice IL-33 expression was assessed in lung sections from Sugen/Hypoxia (SuHx) and control mice. Immunostaining for VE-Cadherin (VE-Cad), DAPI, and IL-33 showed significantly increased IL-33 (red) in ECs of pulmonary vessels in SuHx mice compared to normoxic controls, confirming IL-33 upregulation under hypoxia. To explore IL-33's role in PAH pathophysiology, its expression was evaluated in human PAECs. IL33 mRNA and secreted IL-33 protein levels were significantly elevated in PAH-derived PAECs compared to controls (Figure 1C, E). Analysis of IL-33 downstream signaling revealed increased *MYD88* and *IL1RAP* mRNA expression in PAH PAECs (Figure 1D). Western blot analysis further confirmed upregulated IL-33 and its receptor accessory protein IL-1RAcP, reinforcing the transcriptional data and supporting IL-33 pathway activation in PAH (Figure 1F). These findings indicate enhanced activation of IL33 signaling in the context of PAH.

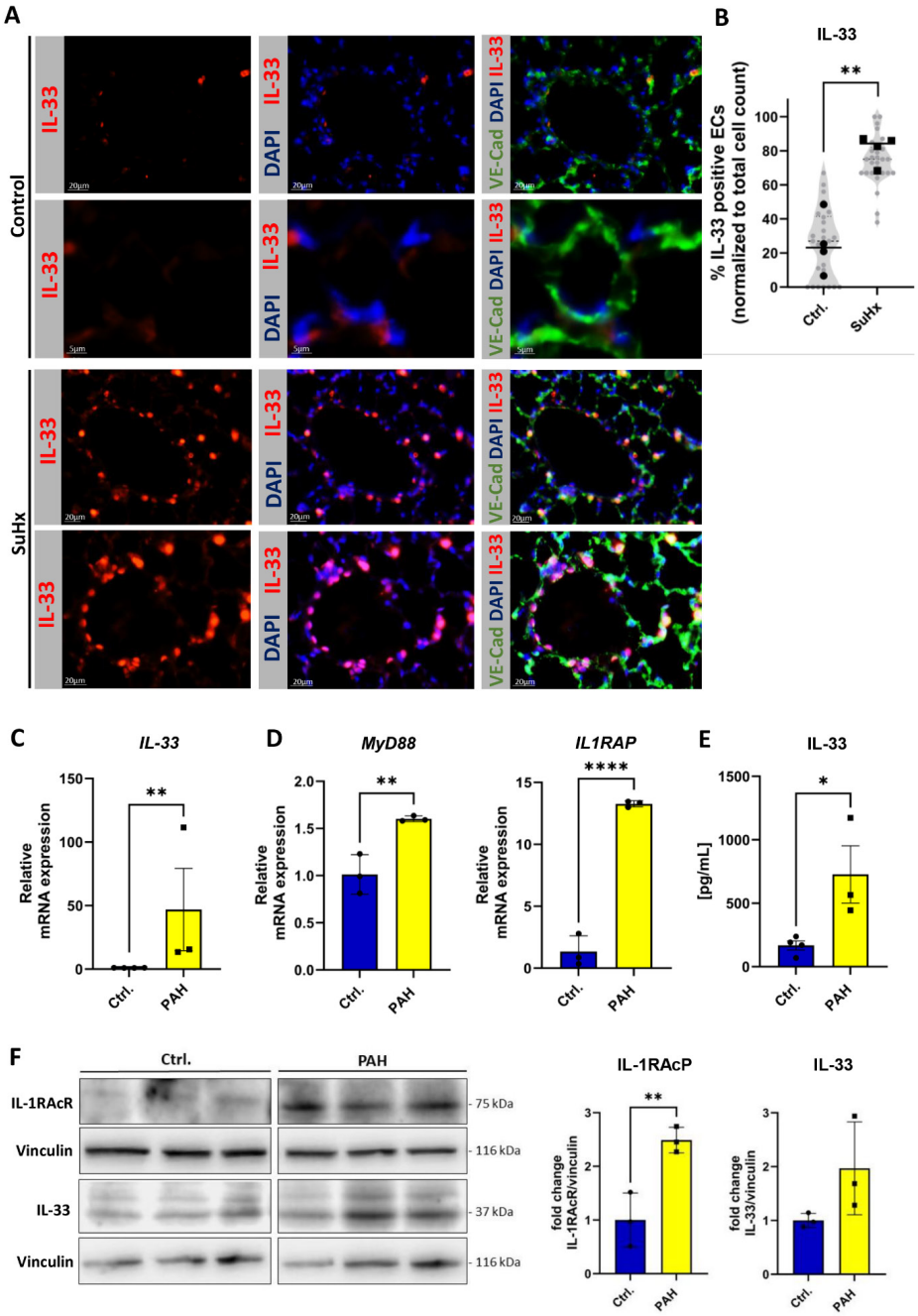

Figure 1. IL-33 expression is increased in human PAEC from PAH patients *in vitro* and pulmonary vessels of Sugen/Hypoxia mice *in vivo*. (A) Representative immunohistochemical images of IL-33, VE-Cadherin, and DAPI in lung sections from normoxic and Su/Hx-treated

mice (n=4). (B) Quantification of IL-33 and VE-Cad co-expression in >25 pulmonary vessels. Grey data points represent individual vessels, black data points show the average per animal. (C, D) *IL33, MyD88,* and *IL1RAP* gene expression in PAH PAEC compared to healthy controls (N=3). (E) Soluble IL-33 levels in PAH PAEC supernatants vs. controls (N=3). (F) Immunoblotting and quantification for IL-33 and IL-1RAcR in PAH PAEC vs. controls (N=3). Statistical analysis: unpaired Student's *t*-test; $p<0.05$, $^{*}p<0.01$, $^{***}p<0.0001$. Data shown as mean ± SD.

BMP9 protects from IL-33-induced EndMT and induces sST2 expression in PAEC

EndMT is a key feature of endothelial dysfunction in PAH. While IL-6 primes PAH MVECs for EndMT under prolonged BMP9 exposure[8], IL-33 also induces EndMT during tissue regeneration[9,18]. We investigated whether IL-33 alone is sufficient to induce EndMT in PAECs or if BMP9 modulates this response. BMP9 alone had no phenotypic effects on control PAECs, but IL-33 stimulation significantly reduced endothelial marker CD31 and increased mesenchymal marker SM22α, indicating EndMT. However, BMP9 co-treatment maintained a quiescent endothelial phenotype, preventing IL-33-induced EndMT (Figure 2A). Given BMP9's protective role, we next examined its interaction with the IL-33/ST2 axis and TGF-β/BMP signaling pathways. As TGF-β ligands typically exhibit slower signaling kinetics than BMPs, a 16-hour stimulation, commonly used to assess TGF-β responses in ECs, was applied. To allow direct comparison with the more rapid kinetics of BMP signaling, we additionally performed 3h stimulations with TGF-β1 and Activin A. In both cases, TGF-β1 and Activin A did not alter sST2 expression, whereas BMP9 and BMP10 significantly upregulated sST2, indicating a specific regulatory effect (Figure 2B, Supplementary Figure S1). Consistently, BMP9 and BMP10 also strongly induced the canonical BMP target genes ID1 and ID3 (Figure 2C), confirming their activity under these conditions.

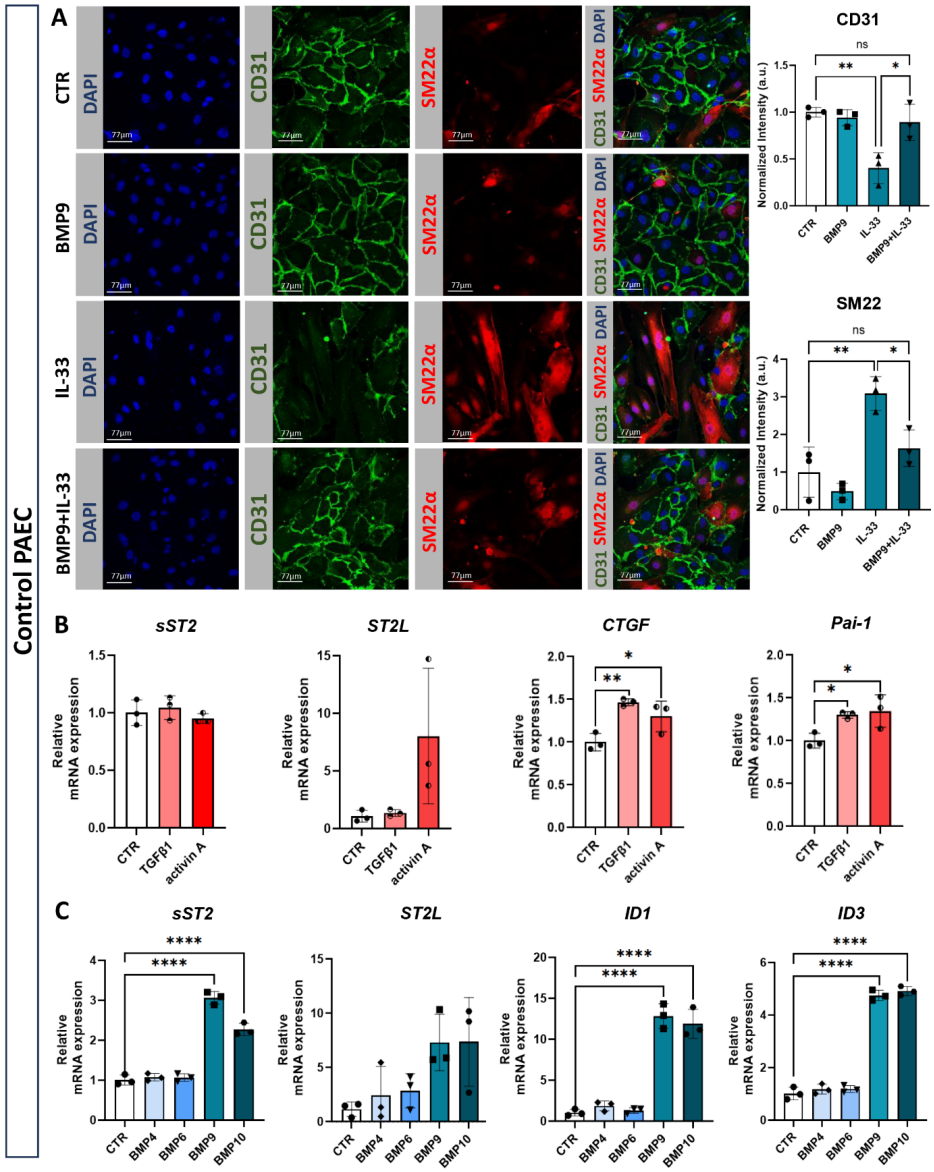

Figure 2. BMP9 protects from IL-33-induced EndMT and induces sST2 expression in control PAEC *in vitro*. (A) Representative immunofluorescent staining of PAEC for CD31 (endothelial marker), SM22α (mesenchymal marker), and DAPI (nuclei). Cells were treated with BMP9 (1 ng/mL), IL-33 (100 ng/mL), both, or left untreated (CTR) for 3 days. Bar graphs show CD31 and SM22α intensity quantification. (B) *sST2, ST2L, CTGF*, and *PAI-1* gene expression in PAECs after 16h stimulation with TGF-β (1 ng/mL), Activin A (50 ng/mL), or untreated (CTR). (C) *sST2, ST2L, ID1*, and *ID3* gene expression in PAECs after 3h stimulation with BMP4 (50 ng/mL), BMP6 (50 ng/mL), BMP9 (1 ng/mL), BMP10 (1 ng/mL), or untreated (CTR) (N=3). Statistical analysis: one-way ANOVA with Tukey's post-hoc test; *p<0.05, **p<0.01, ****p<0.0001. Data shown as mean ± SD.

BMP9 induces sST2 expression via Alk1 signaling in a dose-and time dependent manner

Given the strong BMP9-induced sST2 upregulation in PAECs (Figure 2C), we further characterized this effect across multiple donors. BMP9 significantly increased both sST2 mRNA and secreted protein levels, without affecting IL-33 mRNA expression or secretion (Figure 3A, Supplementary Figure S2A). This induction was dose-dependent, with minimal upregulation observed at 0.1 ng/mL BMP9 and a gradual increase at 1 and 5 ng/mL on both mRNA and protein levels (Figure 3B, Supplementary Figure S2B). Time-course analysis revealed no induction after 1-hour stimulation with 1 ng/mL BMP9, while robust sST2 expression was evident at 3 and 24 hours, indicating a temporally regulated response. In ECs, BMP9 displays a high affinity for ALK1, which forms a signaling complex with the type II receptor BMPR2[19]. Therefore, we tested whether ALK1 activity mediates BMP9-induced sST2 expression. Pre-treatment with a selective kinase inhibitor, LDN-193189 (120 nM), significantly reduced the transcriptional activation of *ID1* and *ID3*, but did not affect BMP9-induced sST2 upregulation at 3h. At 24h, however, LDN significantly reduced sST2 transcript levels (Figure 3D). As expected, ID1 expression was minimal at 24 hours due to its early response kinetics (Supplementary Figure S2D). Importantly, LDN also attenuated BMP9-induced sST2 protein secretion and mRNA expression in a concentration-independent manner (Figure 3E and Supplementary Figure S2E). LDN-193189 is a broad ATP-competitive inhibitor that blocks several BMP/TGF-β type I receptors, including ALK1, ALK2, ALK3, and ALK6, but its effectiveness can vary depending on the cell type. To directly test which receptor mediates BMP9-induced sST2 expression, we performed siRNA knockdown of ALK1 and endoglin (ENG). Silencing ALK1 completely blocked sST2 mRNA induction by BMP9 at 3 hours, whereas knockdown of ENG had no effect (Figure 3F). The efficiency of ALK1 and ENG knockdown was confirmed by qPCR, and siALK1 also inhibited BMP9 target gene expression (Supplementary Figure S2F). These results confirm that BMP9 induces sST2 expression specifically through ALK1 and independently of endoglin.

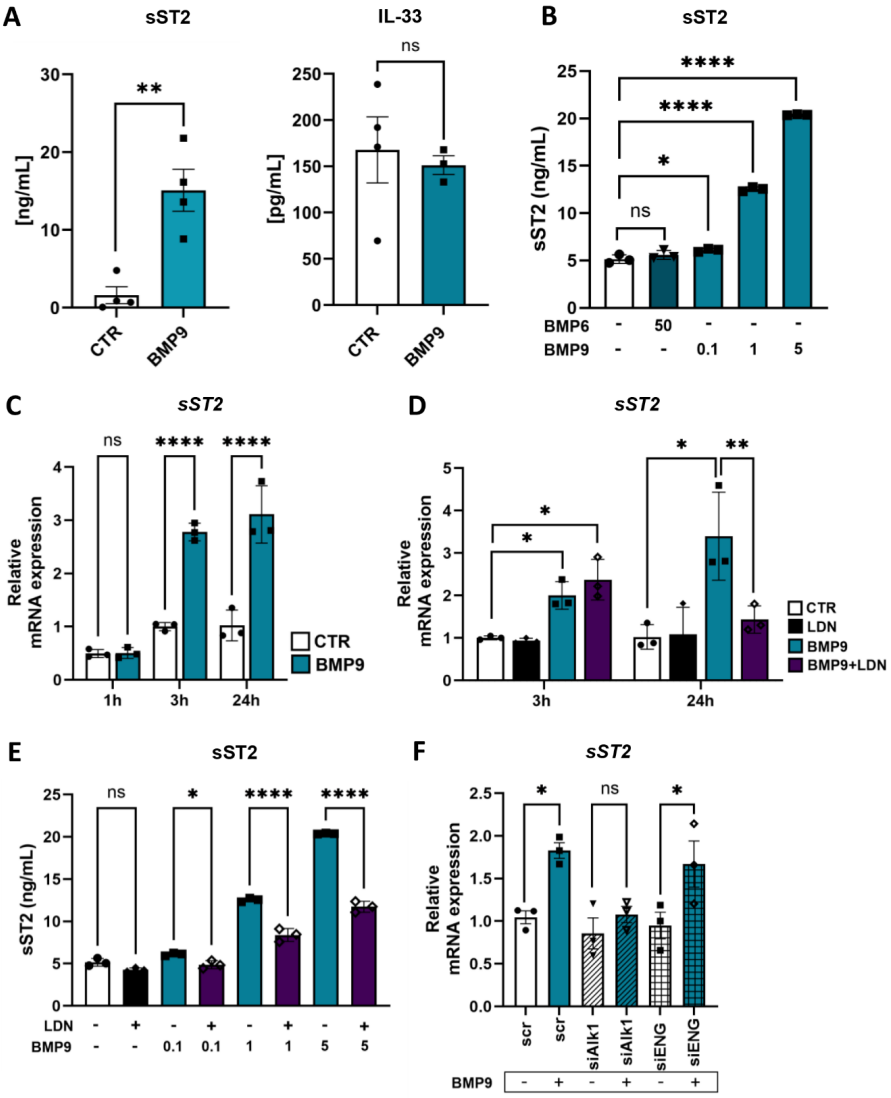

Figure 3. BMP9 induces sST2 expression *in vitro* in PAECs via Alk1 signaling in a dose-and time-dependent manner. (A) Secreted protein levels of sST2 and IL-33 in PAEC supernatants after 24-hour BMP9 (1 ng/mL) stimulation compared to unstimulated controls. Each data point represents three biological replicates per donor (B) Dose-dependent increase in sST2 protein secretion following 24-hour stimulation with 0.1, 1, or 5 ng/mL BMP9. (C) Time-dependent induction of sST2 mRNA expression after 1, 3, or 24 hours of BMP9 stimulation (1 ng/mL). (D) sST2 mRNA expression in PAECs pre-treated with LDN-193189 (120 nM, 30 min) followed by BMP9 (1 ng/mL) stimulation for 3 or 24 hours. (E) Secreted sST2 protein levels following 24-hour stimulation with increasing concentrations of BMP9 in the presence or absence of LDN-193189 (120 nM). (F) sST2 mRNA expression in PAECs transfected with siRNA targeting ALK1 or ENG and stimulated with BMP9 (1 ng/mL, 3h). Statistical analysis:

(A) unpaired Student's *t*-test; (B, E-F) one-way ANOVA with Tukey's post-hoc test for multiple comparisons; (C-D) two-way ANOVA with Tukey's post-hoc testing for multiple comparisons. *p<0.05, **p<0.01, ***p<0.001, ****p<0.0001, ns = not significant. Data shown as (A) mean ± SEM, (B-F) mean ± SD.

BMP9 prevents IL-33-induced EndMT equally effective as recombinant soluble ST2 and inhibits IL-33 target gene expression

Since BMP9 upregulates sST2 (Figure 3A, C), we examined whether this mechanism mediates BMP9's protection against IL-33-induced EndMT. Immunofluorescent staining confirmed that IL-33 reduced CD31 and increased SM22α, indicating EndMT, while pre-treatment with BMP9 or recombinant soluble ST2 (rsST2) prevented these changes, preserving endothelial integrity (Figure 4A). Notably, BMP9 was more effective than anti-ST2L antibody treatment in preventing IL-33-induced EndMT, as indicated by better-preserved VE-Cad expression (Supplementary Figure S3). To investigate whether BMP9's protection extends beyond sST2 induction, we analyzed IL-33 downstream signaling. Western Blot showed that IL-33 treatment led to a time-dependent increase in p-p38 and p-IκBα, indicating pathway activation. While rsST2 slightly reduced their phosphorylation, BMP9 nearly abolished their IL-33-induced activation (Figure 4B-C). In parallel BMP9 significantly reduced IL-33 target genes expression (*MyD88*, *IL1RAP*, and *IL8*) within 3h of treatment (Figure 4D). Thus, BMP9 not only induces sST2 expression but also suppresses IL-33 signaling, further protecting PAECs from IL-33-induced EndMT.

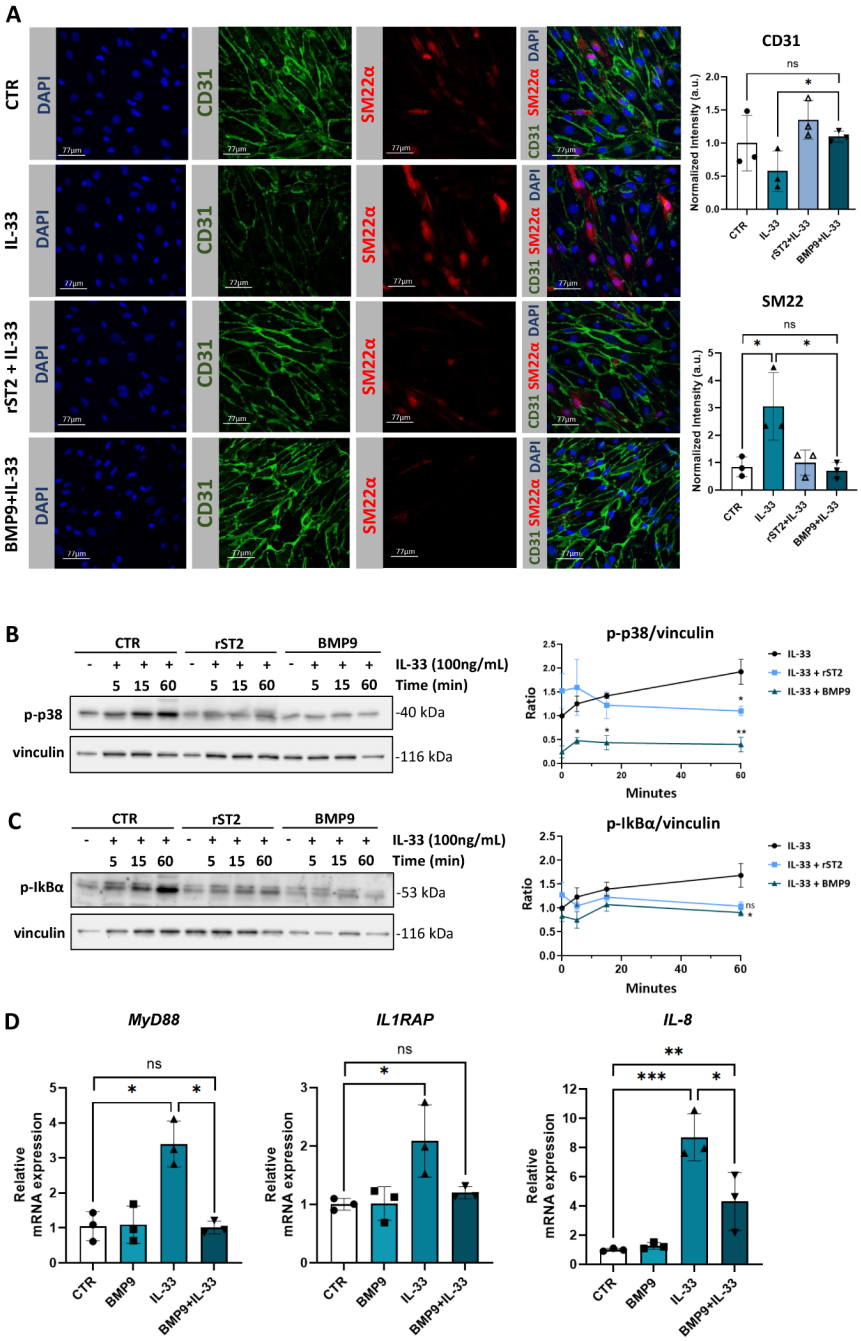

Figure 4. BMP9 prevents IL-33-induced EndMT in PAECs *in vitro* similarly to recombinant soluble ST2, thereby inhibiting IL-33 target gene expression. (A) Representative immunofluorescent staining of for CD31 (endothelial marker), SM22α (mesenchymal marker),

and DAPI (nuclei). Cells were pre-treated with BMP9 (1 ng/mL, 3h) or recombinant soluble ST2 (rsST2, 1 μg/mL, 30 min) before IL-33 (100 ng/mL) stimulation for 3 days. Bar graphs show CD31 and SM22α intensity quantification. (B-C) Representative immunoblots of p-p38 and p-IκBα in PAECs pre-treated overnight with BMP9 (1 ng/mL), rST2 (1 μg/mL, 30 min), or left untreated before IL-33 (100 ng/mL) stimulation for 5, 15, or 60 min. Densitometric analysis was performed using ImageJ, with protein levels normalized to vinculin and expressed as fold change relative to the 0-min control. (D) *MyD88, IL1RAP* and *IL-8* gene expression in PAEC pre-treated with BMP9 (1 ng/mL, 3h) before IL-33 (100 ng/mL, 24h) stimulation or left untreated (CTR) (N=3). Statistical analysis: one-way ANOVA (A, D) or two-way ANOVA (B, C) with Tukey's post-hoc test; $p<0.05$, $^{*}p<0.01$, $^{**}p<0.001$, ns = not significant. Data shown as mean ± SD (A, D) or mean ± SEM (B, C).

BMP9 protects from IL-33-induced EndMT and induces sST2 expression in PAEC from PAH patients

ECs from PAH patients exhibit altered BMP9 and IL-6 responses compared to control cells[9]. Prolonged BMP9 exposure in PAH MVECs induces EndMT-like changes, including VE-Cad loss and increased SM22α expression. To determine whether BMP9 protects PAH PAECs from IL-33-induced EndMT, we conducted similar experiments. As in control PAECs, BMP9 alone had no effect, while IL-33 significantly reduced CD31 and increased SM22α, indicating EndMT. However, BMP9 co-treatment preserved CD31 and suppressed SM22α expression, confirming BMP9's protective role in PAH PAECs (Figure 5A). To further assess BMP9's role in modulating the IL-33/ST2 axis, we examined sST2 expression in PAH PAECs and MVECs. Neither TGF-β1 nor Activin A induced sST2 expression in PAH PAECs (Figure 5B), control MVECs, or PAH MVECs (Supplementary Figure S4A+C). In contrast, BMP9 and BMP10 significantly upregulated sST2 (Figure 5C, Supplementary Figure S4B+D), highlighting their distinct role in IL-33/ST2 pathway regulation across pulmonary ECs in PAH pathogenesis.

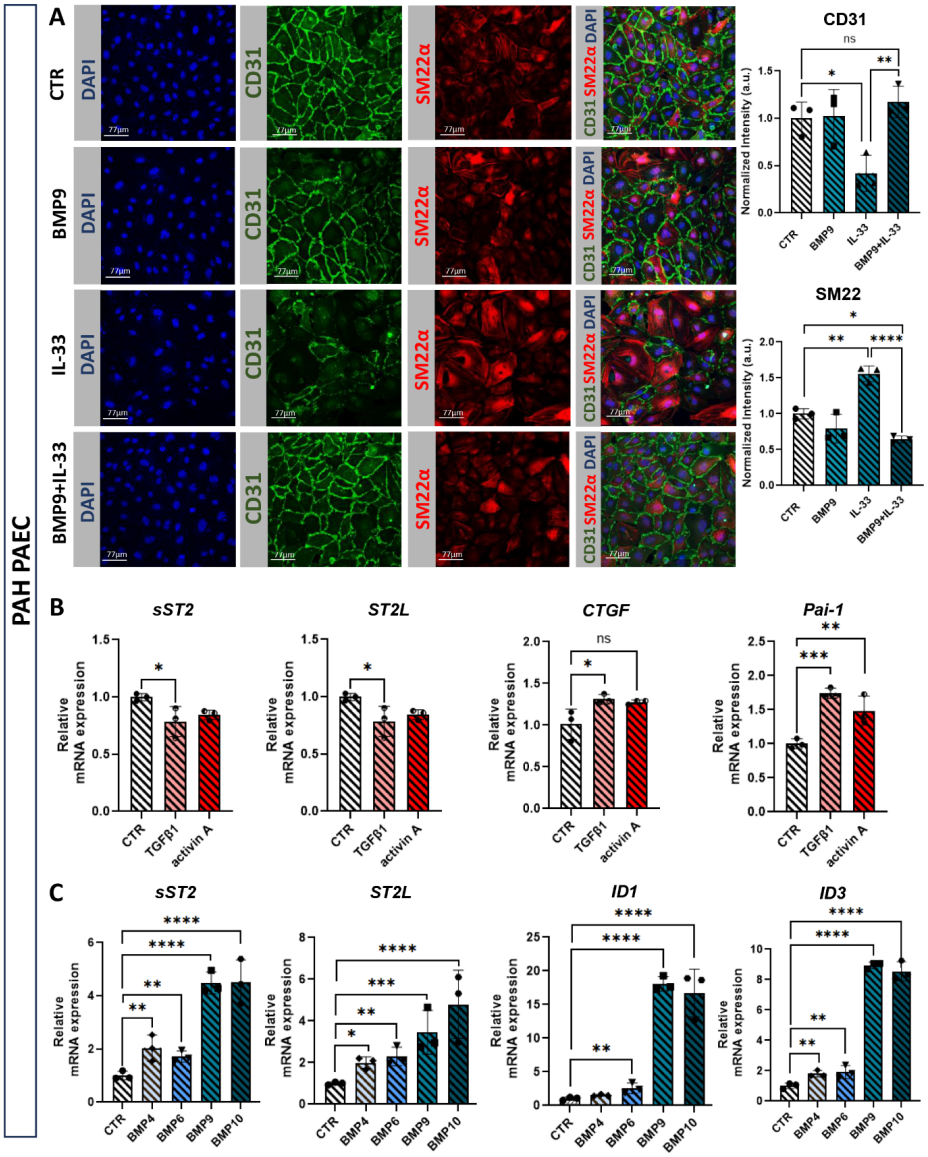

Figure 5. BMP9 protects from IL-33-induced EndMT and induces sST2 expression in PAEC from PAH patients *in vitro*. (A) Representative immunofluorescent staining of PAH PAEC for CD31 (endothelial marker), SM22α (mesenchymal marker), and DAPI. Cells were treated with BMP9 (1 ng/mL), IL-33 (100 ng/mL), both, or left untreated (CTR) for 3 days. Bar graphs show quantification of CD31 and SM22α intensity. (B) *sST2, ST2L, CTGF* and *Pai-1* gene expression in PAH PAECs s after 16h stimulation with TGF-β (1 ng/mL), Activin A (50 ng/mL), or untreated (CTR). (C) *sST2, ST2L, ID1* and *ID3* gene expression in PAH PAECs after 3h stimulation with BMP4 (50 ng/mL), BMP6 (50 ng/mL), BMP9 (1 ng/mL), BMP10 (1 ng/mL), or untreated (CTR) (N=3). Statistical analysis: one-way ANOVA with Tukey's post-hoc test; $p<0.05$, *$p<0.01$, **$p<0.001$, ***$p<0.0001$. Data shown as mean ± SD.

IL-33 expression is upregulated in pulmonary vessels of PAH patients and circulating sST2 correlates with BMP9 levels in stratified PAH Groups

Since our *in vitro* findings suggest a crosstalk between BMP9 and sST2 in pulmonary EC implicated in the pathogenesis of PAH, we sought to investigate whether similar correlations are evident *in vivo.* Therefore, we measured circulating levels of sST2 and BMP9 in 79 patients with PAH. The median age of this cohort was 67 years, 53% were female, and 63% were classified as New York Heart Association (NYHA) class III or IV. Of these, 20% had pathogenic BMPR2 mutations (hereditary PAH), while the rest had idiopathic PAH. Median pulmonary artery pressure (PAP) was 48 mmHg, and median pulmonary vascular resistance (PVR) was 772 dyne/s/cm^{-5} (Table 1).

Table 1. Baseline characteristics.

Participants (n)	**N=79**
Female, %	53
Age (years)	67 [61-69]
Idiopathic PAH (%)	80
Heritable PAH (%)	20
Serum NT-proBNP, ng.L^{-1}	1377 [907-1810]
BMI (kg.m^{-2})	25.6 [24.9-26.5]
mPAP, mmHg	48 [45-51]
PVR, dyne.s.cm^{-5}	772 [642-856]
Cardiac Index, L.min.m^{2}	2.08 [1.94-2.30]
RAP, mmHg	7 [6-8]
6MWD, m	300 [260-357]
NYHA FC, %	
I	5
II	31
III	49
IV	14
BM9, pg.mL-1	1377 [907-1810]
sST2, ng/mL -1	19.6 [14.5-24.3]

BMI, body mass index; mPAP, mean pulmonary arterial pressure; PVR, pulmonary vascular resistance; RAP, right atrial pressure; NYHA FC, New York Heart Association functional class; 6MWD, 6-minute walking distance. Results are expressed as median [95% confidence interval]

sST2 levels were significantly elevated in male patients, individuals >67 years, and those classified as NYHA class III-IV (Figure 6A), while BMP9 levels showed no significant differences across groups (Supplementary Figure S5A). In males and patients >67 years, circulating sST2 positively correlated with BMP9 (Figure 6B), but this association was absent in females, younger patients, and those with NYHA class I-II (Supplementary Figure S5B). Despite elevated sST2 levels in NYHA III-IV patients, no significant correlation with BMP9 was found. Our results described above suggest that increased levels of IL-33 are associated with the pathogenesis of PAH and that its inhibition may represent a viable therapeutic strategy to mitigate endothelial remodeling in PAH patients. To confirm increased IL-33 expression in PAH, we performed immunofluorescence on lung sections from control and IPAH patients. α-SMA expression was elevated in the microvessels of IPAH patients due to muscularization of the pre-capillary arteries, consistent with prior reports[20]. Moreover, IL-33 expression was significantly higher in the ECs of pulmonary vessels in IPAH patients compared to healthy controls.

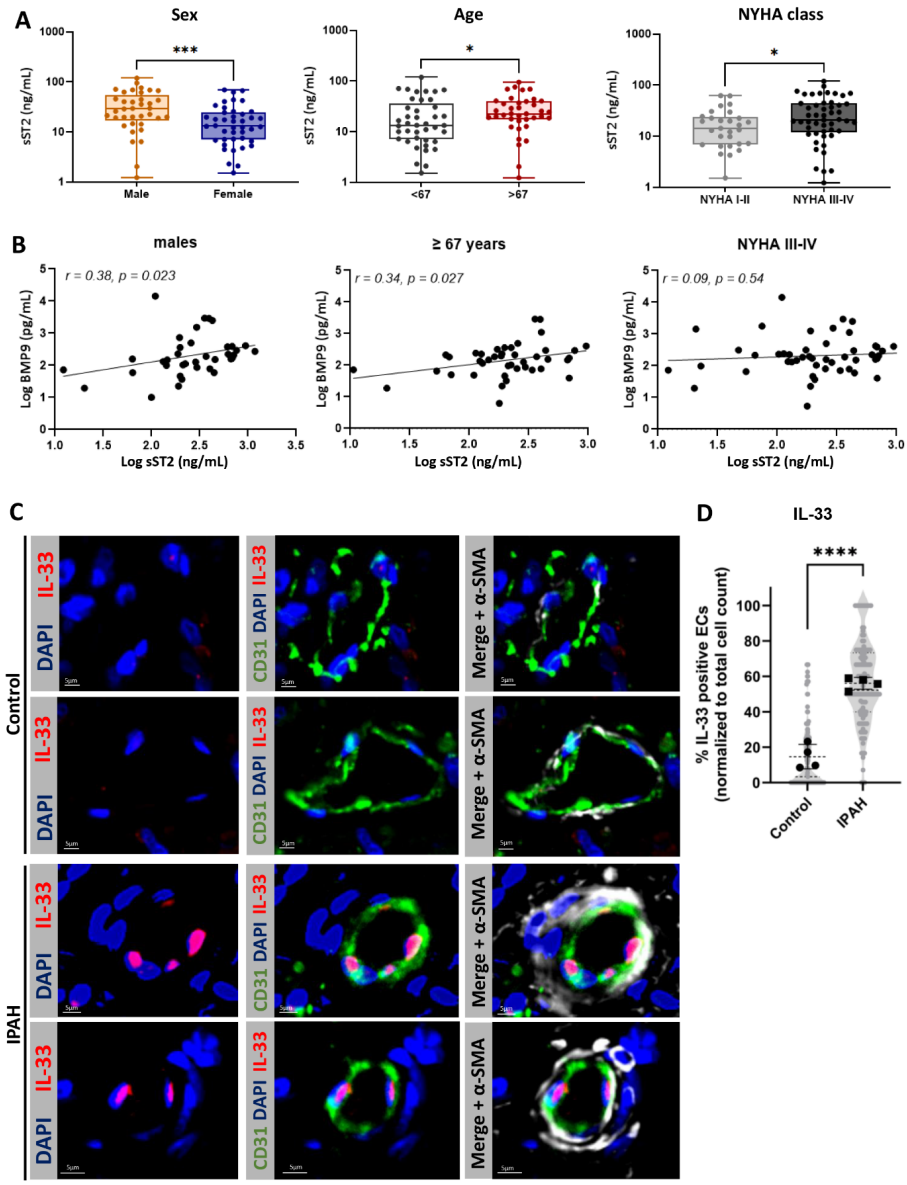

Figure 6: IL-33 expression is upregulated in pulmonary vessels of PAH patients, and circulating sST2 correlates with BMP9 levels in stratified PAH Groups. (A) Circulating levels of sST2 in PAH patients stratified by sex, age, and NYHA class (N=79). (B) Correlation between circulating sST2 and BMP9 in sub-stratified groups with high circulating sST2 levels. (C) Representative images of immunohistochemical staining for IL-33, CD31, α-SMA, and DAPI in lung sections from PAH patients or healthy controls (n = 4). (D) Quantification of IL-33$^+$ ECs per vessel, normalized to total ECs, from ≥30 vessels across 4 individuals per condition. Statistical analysis: (A) Mann-Whitney test on log-transformed values, (B) Spearman correlation, (D) unpaired t-test; p<0.05, *p<0.01, **p<0.001, ***p<0.0001. Data shown as mean ± SD.

Discussion

This study demonstrates that IL-33 is significantly upregulated in PAECs from PAH patients and in pulmonary vessels of Su/Hx mice, contributing to endothelial dysfunction via EndMT. BMP9 counteracts IL-33-induced EndMT by inducing sST2, thereby neutralizing IL-33 signaling, a mechanism observed in both control and PAH-derived PAECs. We show that BMP9-mediated sST2 induction is ALK1-dependent and occurs in a dose- and time-dependent manner, requiring the presence of ALK1 receptor and sustained receptor kinase activity. Furthermore, IL-33 expression was significantly elevated in pulmonary ECs of IPAH patients. In a cohort of PAH patients, circulating sST2 levels were higher in males, individuals >67 years, and more severe PAH cases, with a positive correlation between sST2 and BMP9 levels in these stratified groups.

IL-33 has been implicated in both protective and pathological roles across cardiovascular and respiratory diseases. While it is cardioprotective in conditions like atherosclerosis, its upregulation in respiratory diseases, including COPD and asthma, is linked to disease severity[21,22]. In PAH, recent evidence suggests that prolonged IL-33 administration increases right ventricular pressure in mice, further supporting that IL-33 contributes to the progression of PAH pathogenesis[23]. However, the exact source and regulation of IL-33 in PAH remain poorly understood. It is thought to originate from various lung cell types, including epithelial, endothelial, and possibly activated immune cells. Additionally, the factors responsible for IL-33 upregulation, such as inflammation, hypoxia, or mechanical stress, require further exploration. Elevated circulating sST2 levels have been described by numerous clinical studies as a robust predictor of mortality in patients with heart failure and left ventricular systolic dysfunction[24]. High levels of sST2 are then often associated with disease progression due to neutralization of the protective effects of IL-33 in the heart, causing maladaptive remodelling like fibrosis. In PAH, sST2 has been proposed as a prognostic biomarker with elevated levels correlating with right ventricular dysfunction and increased mortality risk[25]. Elevated circulating sST2 levels may originate from myocardial stress as well as from vascular remodelling in the pulmonary arteries[26]. High sST2 levels might also reflect a compensatory mechanism to counteract the detrimental effects of elevated IL-33 in the lungs. The observed sex- and age-related differences in sST2 levels align with previous findings in cardiovascular diseases, where testosterone has been shown to increase circulating sST2[27]. The correlation between BMP9 and sST2 in specific patient subgroups suggests a context-dependent interaction, possibly linked to advanced disease stages or systemic

vascular dysfunction. However, this correlation was absent in the broader cohort, likely due to patient heterogeneity.

Mechanistically, our data reveal that BMP9 induces sST2 expression in an ALK1-dependent manner. While short-term LDN-193189 treatment failed to block sST2 induction at 3h, siRNA-mediated ALK1 knockdown abolished the response, demonstrating that ALK1 is essential for transcriptional activation. BMP9 triggered sST2 expression in a dose-dependent manner beginning at 0.1 ng/mL, consistent with its high-affinity interaction with ALK1, while BMP6, which primarily signals via ALK2, had no effect. Together, these findings indicate that BMP9 induces sST2 expression through ALK1, and suggest that canonical ALK1 signaling may activate a downstream regulatory mechanism that sustains or stabilizes sST2 expression beyond the initial transcriptional trigger. The partial insensitivity to LDN-193189 at early time points likely reflects context-specific limitations in blocking ALK1 activity in PAECs, rather than true receptor independence.

Despite these important insights, our study has some limitations. The lack of *in vivo* validation for BMP9-IL-33-sST2 interactions limits our mechanistic understanding. Additionally, IL-33 was undetectable in patient plasma, suggesting its local sequestration or rapid degradation. The inability to distinguish between sST2 and the transmembrane isoform ST2L remains a technical challenge, and addressing this gap would enhance our ability to fully elucidate the distinct roles of sST2 and ST2L in cellular and physiological contexts in PAH.

It is important to acknowledge that the IL-33/ST2 signaling axis exhibits considerable biological complexity that complicates *in vitro* investigation. IL-33 acts both as a nuclear chromatin-associated factor and as a secreted cytokine, with its extracellular activity being highly context-dependent and influenced by factors such as proteolytic processing, oxidative environment, and cellular origin[28]. While sST2 is widely recognized as a soluble decoy receptor neutralizing IL-33 by preventing its interaction with the membrane-bound ST2L, recent hypotheses suggest that sST2-IL-33 complexes might stabilize IL-33 by protecting it from oxidative inactivation or proteolytic cleavage, potentially extending its half-life[29]. However, current evidence does not convincingly demonstrate a functional role for these complexes beyond IL-33 sequestration. Moreover, the low abundance, rapid oxidation, and instability of circulating IL-33 pose technical challenges for its reliable detection and quantification, further limiting mechanistic insight. Our findings are interpreted within the current understanding of sST2 acting as an inhibitor of IL-33 signaling. Nonetheless,

we acknowledge that alternative or non-canonical mechanisms may contribute to BMP9's modulation of IL-33-induced EndMT and merit further investigation.

Additionally, our patient-derived PAECs were obtained from patients at advanced disease stages who had been exposed to a combination of therapeutic drugs for several years. In contrast, blood samples were collected at diagnosis, potentially influencing interpretations. Therapeutically, BMP9 has been explored as a PAH treatment due to its ability to enhance BMPR2 signaling[17]. However, its effects are highly context-dependent, with evidence suggesting both protective and pathological roles, including EndMT induction in PAH MVECs. The complexity of BMP9 signaling, including its context-dependent effects on endothelial function and potential to induce EndMT, raises concerns about its therapeutic application in PAH. Given these complexities, alternative approaches that modulate vascular remodeling without the potential drawbacks of BMP9-based therapies are of great interest. One such advancement is sotatercept, an ACVRIIA-Fc ligand trap against activins and GDFs that restores the balance between the pro-proliferative activin pathway and the anti-proliferative BMP pathway in the pulmonary arterial circulation, demonstrating significant clinical benefits in improving exercise capacity and reducing the risk of clinical worsening[30]. Alternative strategies, such as IL-33 inhibition, may offer a more targeted approach to prevent endothelial dysfunction without the complexities associated with BMP9 signaling. Monoclonal antibodies targeting IL-33, such as Tozorakimab and Itepekimab, are currently in clinical trials for COPD (NCT05166889 and NCT05158387), asthma (NCT04570657), and acute respiratory failure (NCT05624450), and could be repurposed for PAH. Additionally, therapeutic modulation of sST2 or ST2L could refine IL-33 activity, though no selective blocking agents currently exist for these isoforms. In addition to this limitation, the restricted availability of primary patient-derived materials compromised our ability to perform experiments across all endothelial cell types, including MVECs from PAH patients. However, the observed induction of sST2 by BMP9 in different ECs suggests that our findings may be broadly applicable.

In summary, our findings offer an alternative yet complementary perspective, highlighting the potential of targeting IL-33 signaling as a strategy to mitigate endothelial dysfunction in PAH. Unlike BMP9-based therapies, which have shown both protective and pathological effects depending on the context, IL-33 inhibition could offer a more targeted strategy to prevent EndMT and vascular remodeling. By focusing on IL-33 inhibition, this approach may complement existing strategies while addressing some of the challenges posed by the dual roles of BMP9 in PAH pathogenesis.

Perspectives

This study reveals a previously underappreciated role for IL-33 as a driver of EndMT in PAH, marked by elevated IL-33 expression in both patient-derived ECs and the Su/Hx mouse model. We identified a protective mechanism whereby BMP9 upregulates the decoy receptor sST2, thereby antagonizing IL-33 signaling and mitigating endothelial dysfunction. This BMP9–sST2 axis offers new insight into how vascular homeostasis is preserved in PAH and advances our understanding of cytokine-mediated vascular remodeling.

Therapeutically, our findings position IL-33 inhibition as a promising strategy to counteract EndMT and pathological vascular remodeling in PAH. Monoclonal antibodies targeting IL-33, currently in clinical trials for other inflammatory lung diseases, could potentially be repurposed for PAH, offering a more selective approach that may circumvent the broader and context-dependent action of BMP9-based therapies.

Future research should focus on validating IL-33 inhibition in *in vivo* models of PAH and investigate the broader therapeutic potential of modulating sST2 expression across diverse vascular beds. Elucidating the upstream regulators of sST2 expression and molecular determinants of IL-33 responsiveness in ECs will be important to refine these strategies further. Ultimately, by uncovering this signaling axis, our study paves the way for more targeted and mechanistically informed interventions aimed at halting or reversing vascular remodeling in PAH.

Author's contributions

C.B. conceptualized and designed the experiments. C.B. and E.J.G. performed all experiments. C.B. analyzed the data. R.Q. provided human plasma and analyzed the clinical data. B.N. and P.X. isolated and provided primary cells. H.J.B., P.B.Y., and F.d.M. provided human and mouse materials. G.S.D. supervised the project. C.B. designed the figures and wrote the manuscript. All authors revised and edited the manuscript. G.S.D. and M.J.G. provided resources and funding acquisition.

Acknowledgements

Schematic figures were created with biorender.com (licensed to G.S.D).

Funding

This work was supported by the FWO Scientific Research Network (W0014200N). C.B. and M.J.G. are sponsored by the Netherlands Cardiovascular Research Initiative (the Dutch Heart Foundation, Dutch Federation of University Medical Centers, the Netherlands Organization for Health Research and Development, and the Royal Netherlands Academy of Sciences), PHAEDRA-IMPACT (DCVA), and DOLPHIN-GENESIS (CVON). C.B is sponsored by the European Joint Programme on Rare Diseases and the Company of Biologists. M.J.G. is supported by Regenerative Medicine Crossing Borders (REGMED XB). G.S.D. is supported by the grants Ramón y Cajal RYC2021-030886-I, PID2022-141212OA-I00, and CNS2023-145432 from the Spanish Ministry of Science and Innovation, the BHF-DZHK-DHF, 2022/23 award PROMETHEUS (02-001-2022-0123), and the Foundation Eugenio Rodriguez Pascual (FERP-2023-058). The authors are grateful to the Belgian Pulmonary Hypertension Patient.

References

1. Humbert M, Kovacs G, Hoeper MM, Badagliacca R, Berger RMF, Brida M, Carlsen J, Coats AJS, Escribano-Subias P, Ferrari P, et al. 2022 ESC/ERS Guidelines for the diagnosis and treatment of pulmonary hypertension. Eur Heart J. 2022;43:3618-3731. doi: 10.1093/eurheartj/ehac237
2. Humbert M, Guignabert C, Bonnet S, Dorfmüller P, Klinger JR, Nicolls MR, Olschewski AJ, Pullamsetti SS, Schermuly RT, Stenmark KR, et al. Pathology and pathobiology of pulmonary hypertension: state of the art and research perspectives. Eur Respir J. 2019;53:1801887. doi: 10.1183/13993003.01887-2018
3. Ranchoux B, Antigny F, Rucker-Martin C, Hautefort A, Péchoux C, Bogaard HJ, Dorfmüller P, Remy S, Lecerf F, Planté S, et al. Endothelial-to-mesenchymal transition in pulmonary hypertension. Circulation. 2015;131:1006-1018. doi: 10.1161/circulationaha.114.008750
4. Lane KB, Machado RD, Pauciulo MW, Thomson JR, Phillips JA, 3rd, Loyd JE, Nichols WC, Trembath RC. Heterozygous germline mutations in BMPR2, encoding a TGF-beta receptor, cause familial primary pulmonary hypertension. Nat Genet. 2000;26:81-84. doi: 10.1038/79226
5. Guignabert C, Savale L, Boucly A, Thuillet R, Tu L, Ottaviani M, Rhodes CJ, De Groote P, Prévot G, Bergot E, et al. Serum and Pulmonary Expression Profiles of the Activin Signaling System in Pulmonary Arterial Hypertension. Circulation. 2023;147:1809-1822. doi: 10.1161/circulationaha.122.061501
6. Yan Y, Wang XJ, Li SQ, Yang SH, Lv ZC, Wang LT, He YY, Jiang X, Wang Y, Jing ZC. Elevated levels of plasma transforming growth factor-β1 in idiopathic and heritable pulmonary arterial hypertension. Int J Cardiol. 2016;222:368-374. doi: 10.1016/j.ijcard.2016.07.192
7. Becher C, Wits M, de Man FS, Sanchez-Duffhues G, Goumans MJ. Targeting Soluble TGF-β Factors: Advances in Precision Therapy for Pulmonary Arterial Hypertension. JACC Basic Transl Sci. 2024;9:1360-1374. doi: 10.1016/j.jacbts.2024.04.005
8. Tu L, Desroches-Castan A, Mallet C, Guyon L, Cumont A, Phan C, Robert F, Thuillet R, Bordenave J, Sekine A, et al. Selective BMP-9 Inhibition Partially Protects Against Experimental Pulmonary Hypertension. Circ Res. 2019;124:846-855. doi: 10.1161/circresaha.118.313356
9. Szulcek R, Sanchez-Duffhues G, Rol N, Pan X, Tsonaka R, Dickhoff C, Yung LM, Manz XD, Kurakula K, Kiełbasa SM, et al. Exacerbated inflammatory signaling underlies aberrant response to BMP9 in pulmonary arterial hypertension lung endothelial cells. Angiogenesis. 2020;23:699-714. doi: 10.1007/s10456-020-09741-x
10. Drake LY, Kita H. IL-33: biological properties, functions, and roles in airway disease. Immunol Rev. 2017;278:173-184. doi: 10.1111/imr.12552

11. Liu X, Hammel M, He Y, Tainer JA, Jeng US, Zhang L, Wang S, Wang X. Structural insights into the interaction of IL-33 with its receptors. Proceedings of the National Academy of Sciences of the United States of America. 2013;110:14918-14923. doi: 10.1073/pnas.1308651110

12. Liew FY, Girard J-P, Turnquist HR. Interleukin-33 in health and disease. Nature Reviews Immunology. 2016;16:676-689. doi: 10.1038/nri.2016.95

13. Liu J, Wang W, Wang L, Chen S, Tian B, Huang K, Corrigan CJ, Ying S, Wang W, Wang C. IL-33 Initiates Vascular Remodelling in Hypoxic Pulmonary Hypertension by up-Regulating HIF-1α and VEGF Expression in Vascular Endothelial Cells. EBioMedicine. 2018;33:196-210. doi: 10.1016/j.ebiom.2018.06.003

14. Indralingam CS, Gutierrez-Gonzalez AK, Johns SC, Tsui T, Cannon DT, Fuster MM, Bigby TD, Jennings PA, Breen EC. IL-33/ST2 receptor-dependent signaling in the development of pulmonary hypertension in Sugen/hypoxia mice. Physiol Rep. 2022;10:e15185. doi: 10.14814/phy2.15185

15. Quarck R, Nawrot T, Meyns B, Delcroix M. C-reactive protein: a new predictor of adverse outcome in pulmonary arterial hypertension. J Am Coll Cardiol. 2009;53:1211-1218. doi: 10.1016/j.jacc.2008.12.038

16. Szulcek R, Happé CM, Rol N, Fontijn RD, Dickhoff C, Hartemink KJ, Grünberg K, Tu L, Timens W, Nossent GD, et al. Delayed Microvascular Shear Adaptation in Pulmonary Arterial Hypertension. Role of Platelet Endothelial Cell Adhesion Molecule-1 Cleavage. Am J Respir Crit Care Med. 2016;193:1410-1420. doi: 10.1164/rccm.201506-1231OC

17. Long L, Ormiston ML, Yang X, Southwood M, Gräf S, Machado RD, Mueller M, Kinzel B, Yung LM, Wilkinson JM, et al. Selective enhancement of endothelial BMPR-II with BMP9 reverses pulmonary arterial hypertension. Nat Med. 2015;21:777-785. doi: 10.1038/nm.3877

18. Kenswil KJG, Pisterzi P, Sánchez-Duffhues G, van Dijk C, Lolli A, Knuth C, Vanchin B, Jaramillo AC, Hoogenboezem RM, Sanders MA, et al. Endothelium-derived stromal cells contribute to hematopoietic bone marrow niche formation. Cell stem cell. 2021;28:653-670. e611. doi: 10.1016/j.stem.2021.01.006

19. Cai J, Pardali E, Sánchez-Duffhues G, ten Dijke P. BMP signaling in vascular diseases. FEBS Lett. 2012;586:1993-2002. doi: 10.1016/j.febslet.2012.04.030

20. Tuder RM, Stacher E, Robinson J, Kumar R, Graham BB. Pathology of pulmonary hypertension. Clin Chest Med. 2013;34:639-650. doi: 10.1016/j.ccm.2013.08.009

21. Seki K, Sanada S, Kudinova AY, Steinhauser ML, Handa V, Gannon J, Lee RT. Interleukin-33 prevents apoptosis and improves survival after experimental myocardial infarction through ST2 signaling. Circ Heart Fail. 2009;2:684-691. doi: 10.1161/circheartfailure.109.873240

22. Miller AM, Xu D, Asquith DL, Denby L, Li Y, Sattar N, Baker AH, McInnes IB, Liew FY. IL-33 reduces the development of atherosclerosis. J Exp Med. 2008;205:339-346. doi: 10.1084/jem.20071868

23. Ikutani M, Shimizu S, Okada K, Imami K, Inagaki T, Nakaoka Y, Osada Y, Nakae S. Characterization of long-term interleukin-33 administration as an animal model of pulmonary arterial hypertension. Biochemical and biophysical research communications. 2024;734:150750. doi: 10.1016/j.bbrc.2024.150750

24. Feng Y, He L-q. Soluble ST2: A Novel Biomarker for Diagnosis and Prognosis of Cardiovascular Disease. Current Medical Science. 2024;44:669-679. doi: 10.1007/s11596-024-2907-x

25. Geenen LW, Baggen VJM, Kauling RM, Koudstaal T, Boomars KA, Boersma E, Roos-Hesselink JW, van den Bosch AE. The Prognostic Value of Soluble ST2 in Adults with Pulmonary Hypertension. J Clin Med. 2019;8. doi: 10.3390/jcm8101517

26. Vonk Noordegraaf A, Chin KM, Haddad F, Hassoun PM, Hemnes AR, Hopkins SR, Kawut SM, Langleben D, Lumens J, Naeije R. Pathophysiology of the right ventricle and of the pulmonary circulation in pulmonary hypertension: an update. Eur Respir J. 2019;53:1801900. doi: 10.1183/13993003.01900-2018

27. Coronado MJ, Bruno KA, Blauwet LA, Tschöpe C, Cunningham MW, Pankuweit S, van Linthout S, Jeon ES, McNamara DM, Krejčí J, et al. Elevated Sera sST2 Is Associated With Heart Failure in Men ≤50 Years Old With Myocarditis. J Am Heart Assoc. 2019;8:e008968. doi: 10.1161/jaha.118.008968

28. Sun Y, Pavey H, Wilkinson I, Fisk M. Role of the IL-33/ST2 axis in cardiovascular disease: A systematic review and meta-analysis. PLoS One. 2021;16:e0259026. doi: 10.1371/journal.pone.0259026

29. Sanada S, Hakuno D, Higgins LJ, Schreiter ER, McKenzie AN, Lee RT. IL-33 and ST2 comprise a critical biomechanically induced and cardioprotective signaling system. J Clin Invest. 2007;117:1538-1549. doi: 10.1172/jci30634

30. Hoeper MM, Badesch DB, Ghofrani HA, Gibbs JSR, Gomberg-Maitland M, McLaughlin VV, Preston IR, Souza R, Waxman AB, Grünig E, et al. Phase 3 Trial of Sotatercept for Treatment of Pulmonary Arterial Hypertension. N Engl J Med. 2023. doi: 10.1056/NEJMoa2213558

Supplemental Material

Expanded Materials and Methods

EndMT assay (immunofluorescent staining)

Cells were washed in cold PBS, fixed in 4% paraformaldehyde (20 min, RT), quenched with 2 mg/mL glycine, and permeabilized with 0.2% Triton-X (10 min). Blocking was performed with 5% BSA (Sigma-Aldrich, #A-6003), followed by overnight incubation (4˚C) with primary antibodies against CD31 (R&D Systems, #AF3628), VE-Cadherin (Cell Signaling, #2158), and SM22α (Abcam, #ab14106) in 1% BSA/PBS (working concentrations are stated in supplementary table S3). After washing with 0.5% BSA/0.05% Tween-20 in PBS, samples were incubated at RT (1h, dark) with Alexa-conjugated secondary antibodies. Samples were preserved in ProLong Gold with DAPI (Thermo Fisher) and imaged using a confocal microscope (SP8, Leica Microsystems). ImageJ was used for quantification by measuring VE-cadherin or CD31 and SM22α intensity in ten individual cells from three random locations per well, normalized to unstimulated controls.

Western Blotting

Lysates were prepared in RIPA buffer with protease (Roche, #11836145001) and phosphatase inhibitors (10 mM sodium fluoride, Sigma, #7681-49-4; 400 μM sodium orthovanadate, Sigma, #S6508). Protein concentrations were determined using the Pierce BCA Assay Kit (Thermo Fisher, #23235). Equal protein amounts (20 μg) were mixed with Laemmli buffer, resolved via SDS-PAGE (10% polyacrylamide gels), and transferred onto methanol-activated 45 μm PVDF membranes (Merck Millipore, #IPVH00010). Membranes were blocked (10% non-fat dry milk in TBST, 1h, RT) and incubated overnight (4˚C) with primary antibodies in TBST: phospho-p38 MAPK (Thr180/Tyr182) (Cell Signaling, #4631), phospho-IκB-α (Ser32/36) (Santa Cruz, #sc-101713), and vinculin (Sigma-Aldrich, #V9131) as a loading control (Table S2). After TBST washes, membranes were incubated (1h, RT) with secondary antibodies (1:10,000) anti-mouse HRP (Promega, #W4021) or anti-rabbit HRP (Invitrogen, #31458) in 10% milk/TBST. Detection was performed using ECL (Western Bright Quantum HRP, Advansta, #K-12042-D20), and signals were visualized on a ChemiDoc Imaging System (Bio-Rad).

Immunohistochemical staining

Lung sections were deparaffinized, hydrated, and antigen retrieval was performed by boiling in Antigen Retrieval Buffer (10 mM Tris, pH 9, 1 mM EDTA, 0.05% Tween-20) for 20 min in a pressure cooker. After blocking (1% BSA in 0.1% Tween-PBS), sections were incubated overnight (4°C) with primary antibodies against PECAM-1 (R&D Systems, #AF3628), αSMA (Sigma, #A2547), and IL-33 (R&D Systems, #AF3626-SP) (Table S2). The next day, sections were incubated with Alexa-conjugated secondary antibodies, washed with 0.1% Tween-20/PBS, stained with DAPI (Thermo Scientific, #62248), and mounted with ProLong Gold Antifade (Invitrogen, #P26930). Slides were scanned using the Panoramic 250 slide scanner (3DHISTECH, v1.23) and analyzed in Case Viewer (3DHISTECH, v2.3). IL-33$^+$ endothelial cells (EC) were quantified using ImageJ and normalized to total EC nuclei per vessel.

Supplementary Tables

Supplemental table S1 | Growth factors and cytokines

Growth factors	vendor	Catalogue #
BMP4	R&D systems	314-BP-010/CF
BMP6	R&D R&D systems	507-BP-020/CF
BMP9	R&D R&D systems	3209-BP-010/CF
BMP10	R&D R&D systems	2926-BP-025/CF
Activin A	R&D R&D systems	338-AC-010/CF
TGF-β	R&D R&D systems	240-B-010/CF
IL-33	Prospec	CYT-425
Recombinant ST2	R&D R&D systems	523-ST-100
LDN-193189	Selleckchem	S2618

Supplemental table S2 | Characteristics of PAH patients and control cells

	Control	PAH
Participant (n)	5	7
Female (%)	40	100
Age	72 [69-74]	40 [31-43]
IPAH (%)	NA	57
HPAH (%)	NA	43
mPAP	NA	61.5 [51-76.5]
NT-proBNP	NA	1806 [1375-4020]

Supplemental table S3 | Antibodies

Target antigen	vendor	Catalogue #	Working concentration
Transgelin (SM22a)	Abcam	ab14106	1:250
Pecam (CD31)	R&D systems	AF3628	1:100 (IF), 1:200 (IHC, human)
Ve-Cadherin	Abcam	Ab205336	1:150 (IHC, mouse)
IL-33	R&D systems Proteintech	AF3626 12372-1-AP	1:100 1:800
Alpha-SMA	Sigma	A2547	1:40,000
Alexa Fluor™ Plus 647 Phalloidin	Invitrogen	A30107	1:200
Phosphor-p38 MAPK (Thr180/ Tyr182)	Cell Singling	4631	1:1000
phospho-IκB-α (Ser32/36)	Santa Cruz Biotech.	Sc-101713	1:1000
Phospho-SMAD1(Ser463/465) / SMAD5(Ser463/465)/ SMAD9 (Ser465/467)	Cell Signaling	13820	1:1000
SMAD1	Cell Singling	6944	1:1000
Vinculin	Sigma-Aldrich	V9131	1:1000
Human ST2L/IL-33R	R&D systems	MAB523	1ug/mL
Mouse IgG Isotype Control	R&D systems	MAB002	1ug/mL
Alexa Fluor™ 488	Thermo Fisher	A11055 or A21206	1:250
Alexa Fluor™ 555	Thermo Fisher	A31572	1:250
Alexa Fluor™ 647	Thermo Fisher	A21447	1:250

Supplemental table S4 | Primer sequences for qPCR

Gene	Forward 5' → 3'	Reverse 5' → 3'	bp	Annealing Temp (C°)	Gene Bank No.	Specificity/Notes
ID1	CTGCTCTACGACATGAACGG	GAAGGTCCCTGATGTAGTCGAT	124	60	NM_181353.3, NM_002165.4	No additional specific hits in RefSeq mRNA. Partial mismatch binding observed for ID2 (NM_002166.5).
ID3	CACCTCCAGAACGCAGGTGCTG	AGGGCGAAGTTGGGGCCCAT	99	60	NM_002167.5	Only ID3 mRNA amplified; no off-target products detected in RefSeq mRNA
SMAD6	ACAAGCCACTGGATCTGTCC	ACATGCTGGCGTCTGAGAA	102	60	NM_005585.5	Intended product on SMAD6; matches also to predicted SMAD6 XM variants; no other gene targets.
Serpine1 (Pai-1)	CACAAATCAGACGGCAGCACT	CATCGGGCGTGGTGAACTC	85	60	NM_000602.5; NM_001386460.1; NM_001386458.1; NM_001386463.1; NM_001386464.1; NM_001386461.1; NM_001386465.1; NM_001386466.1	Amplifies SERPINE1 across listed transcript variants; no non-SERPINE1 amplicons detected in RefSeq mRNA.
CCN2 (CTGF)	TTGCGAAGCTGACCTGGAAGAGAA	AGCTCGGTATGTCTTCATGCTGGT	121	60	NM_001901.4	Single intended product on CCN2; no off-target amplicons.
sST2	CTCCAAGTTCATCCCCTCTG	GATCCAAAACCCCATTCTGTT	197	55	NM_003856.4	Forward primer in unique **exon 1** (sST2-specific) Intended amplicon on IL1RL1 **sST2** transcript; no product on ST2L
ST2L	GCACTTTGTTCACCAGATTCT	CCAGGTAGCATATCTCTCCCA	87	55	NM_016232.5	Primers in regions **absent in sST2** Intended product on IL1RL1 **ST2L** transcript; no product on sST2

Supplemental table S4 | Primer sequences for qPCR (continued)

Gene	Forward 5' → 3'	Reverse 5' → 3'	bp	Annealing Temp (C°)	Gene Bank No.	Specificity/Notes
IL-33	GGAGTGCTTTG-CCTTTGGTA	TCATTTGAGGG-GTGTTGAGA	243	55	NM_033439.4 NM_001314044.2 NM_001314045.2 NM_001353802.2	Produces amplicons on multiple IL33 transcript variants only; no non-IL33 amplicons.
MyD88	AAAGAGGTTG-GCTAGAAGGC	CAAGGCGAGTC-CAGAACCA	254	55	NM_001172567.2	Single intended product on MYD88; no off-target amplicons.
IL1RAP	CACTTCTGTGGT-GTGTAGTGA	AATG-CAACTTTGCTG CAATAT	376	55	NM_002182.4; NM_134470.4; NM_001167928.2; NM_001167929.2; NM_001167930.2; NM_001167931.2; NM_001364879.1; NM_001364880.2; NM_001364881.2	Intended product across multiple IL1RAP transcript variants; no non-IL1RAP amplicons.
IL-8	CTGTTAAATCTG-GCAACCCTAGTCT	CAAGGCACAGTG-GAACAAGGA	376	60	NM_000584.4; NM_001354840.3	Intended product on CXCL8 transcript variants; no non-CXCL8 amplicons.
GAPDH	AGCCACATCGCT-CAGACAC	GCCCAATACGAC-CAAATCC	66	60	NM_002046.7; NM_001289746.2; NM_001357943.2; NM_001289745.3	Housekeeping Intended product across GAPDH transcript variants; no non-GAPDH amplicons.
ARP (RPLP0)	CACCATT-GAAATCCTGAGT-GATGT	TGACCAGC-CGAAAGGAGAAG	116	60	NM_001002.4; NM_053275.4	Housekeeping Intended product on RPLP0 (ARP) variants. Primer-BLAST lists isolated **reverse-primer** alignments to unrelated transcripts (e.g., CRB1/ITSN1) but **no paired-primer amplicons**—thus no off-target PCR products.

Supplementary Figures

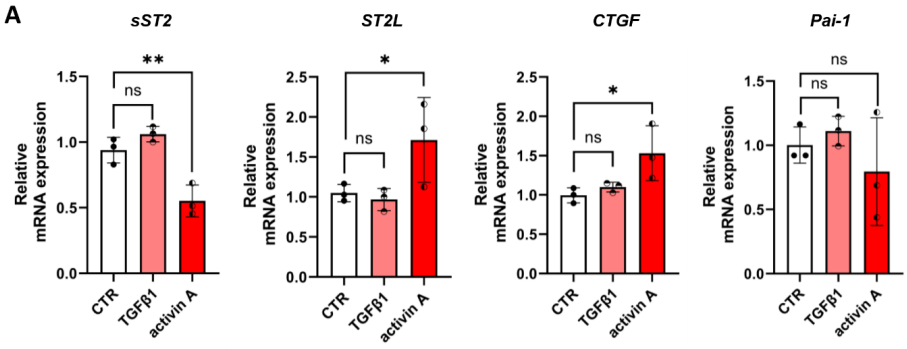

Figure S1. TGF-β ligands do not change sST2 expression in PAECs *in vitro*. (A) Gene expression analysis of *sST2, ST2L, CTGF* and *Pai-1* in control PACEs stimulated for 3h with TGF-β (1ng/mL), ActivinA (50ng/mL) or left untreated (CTR).

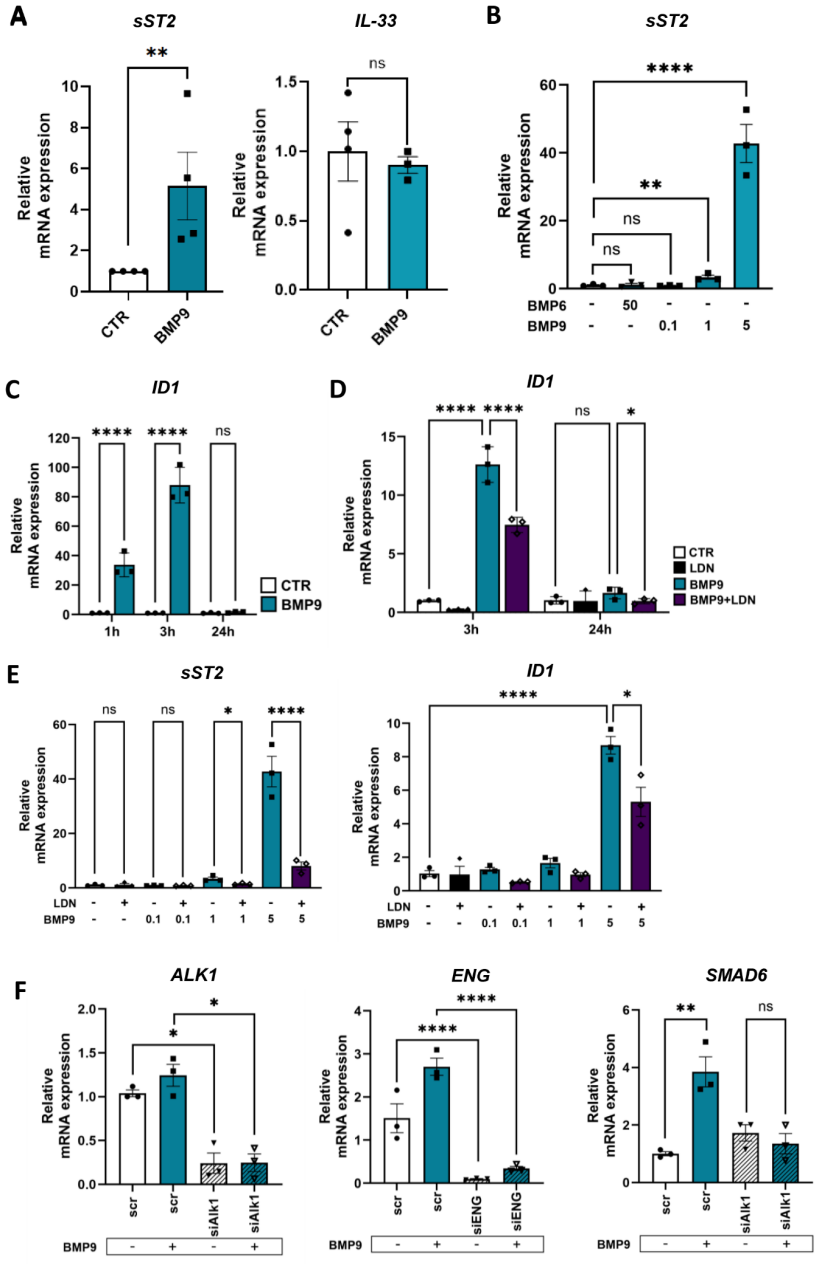

Figure S2. BMP9 induces sST2 expression in a dose- and time-dependent manner through ALK1 signaling in PAECs *in vitro*. (A) mRNA expression of sST2 and IL-33 in PAEC after 3-hour BMP9 (1 ng/mL) stimulation compared to unstimulated controls. Each data point represents three biological replicates per donor (B) Dose-dependent increase in sST2 mRNA following 24-hour stimulation with 0.1, 1, or 5 ng/mL BMP9. (C) mRNA expression of ID after

1, 3, or 24 hours of BMP9 stimulation (1 ng/mL). (D) ID1 mRNA expression in PAECs pre-treated with LDN-193189 (120 nM, 30 min) followed by BMP9 (1 ng/mL) stimulation for 3 or 24 hours. (E) mRNA expression of sST2 and ID1 following 24-hour stimulation with increasing concentrations of BMP9 in the presence or absence of LDN-193189 (120 nM). (F) Alk1, ENG and SMAD6 mRNA expression in PAECs transfected with siRNA targeting ALK1 or ENG and stimulated with BMP9 (1 ng/mL, 3h). Statistical analysis: (A) unpaired Student's t-test; (B, E-F) one-way ANOVA with Tukey's post-hoc test for multiple comparisons; (C-D) two-way ANOVA with Tukey's post-hoc testing for multiple comparisons. *p<0.05, **p<0.01, ***p<0.001, ****p<0.0001, ns = not significant. Data shown as (A) mean ± SEM, (B-F) mean ± SD.

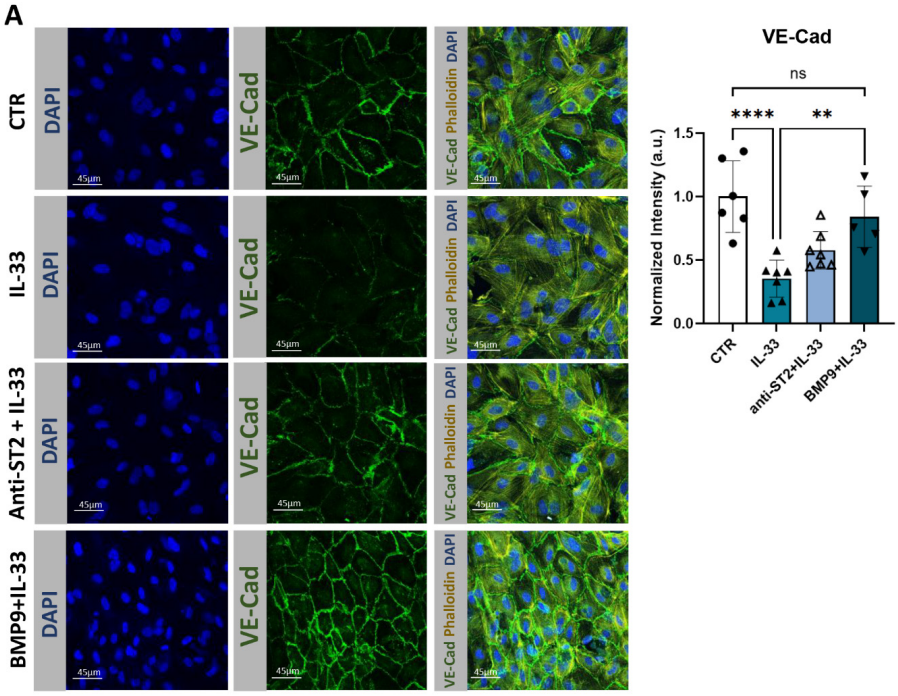

Figure S3. BMP9 rescues IL-33-induced EndMT equally effective anti-ST2L antibody in PAECs *in vitro*. (A) Representative immunofluorescent staining of PAEC for the endothelial marker Ve-Cad, phalloidin, and DAPI. Cells were either left unstimulated, or were pre- treated with BMP9 (1ng/mL) for 3h or anti-ST2L antibody (1ug/mL) for 30 min, followed by stimulation with IL-33 (100ng/mL) for 3 days. Bar graphs represent quantifications of VE-Cad intensity.

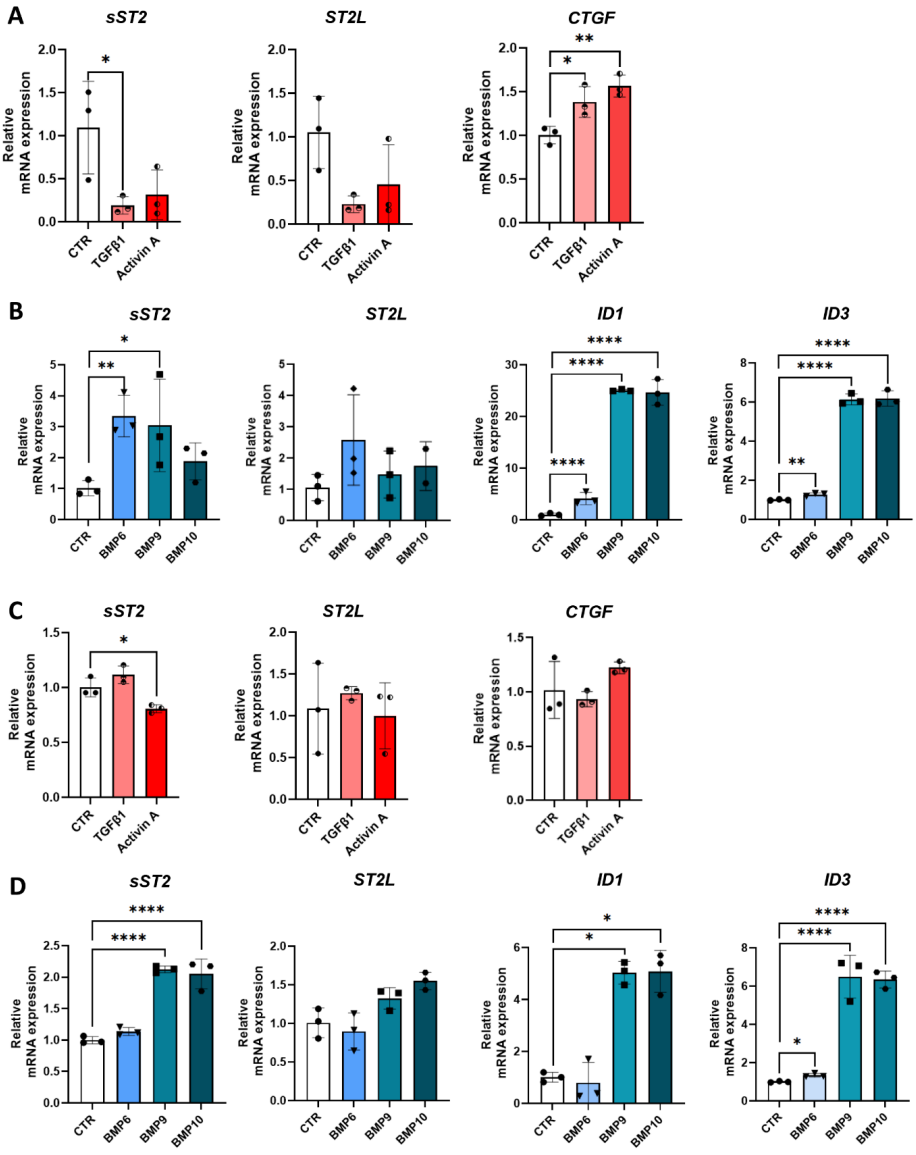

Figure S4. BMP9 induces sST2 expression *in vitro* in control MVECs and MVECs from PAH patients. (A) Gene expression analysis of *sST2, ST2L, CTGF*, and Pai-1 in control MVECs or (C) PAH MVECs stimulated for 16h with TGF-β (1ng/mL), ActivinA (50ng/mL), or left untreated (CTR). (B) Gene expression analysis of *sST2, ST2L, ID1,* and *ID3* in control MVECs or (D) PAH MVECs stimulated for 3h with BMP6 (50ng/mL), BMP9 (1ng/mL), BMP10 (1ng/mL), or left untreated (CTR)(N=3). Statistical differences were tested using one-way ANOVA; *p<0.05, **p<0.01, ***p<0.001, ****p<0.0001. Graphs are displayed as mean + SD.

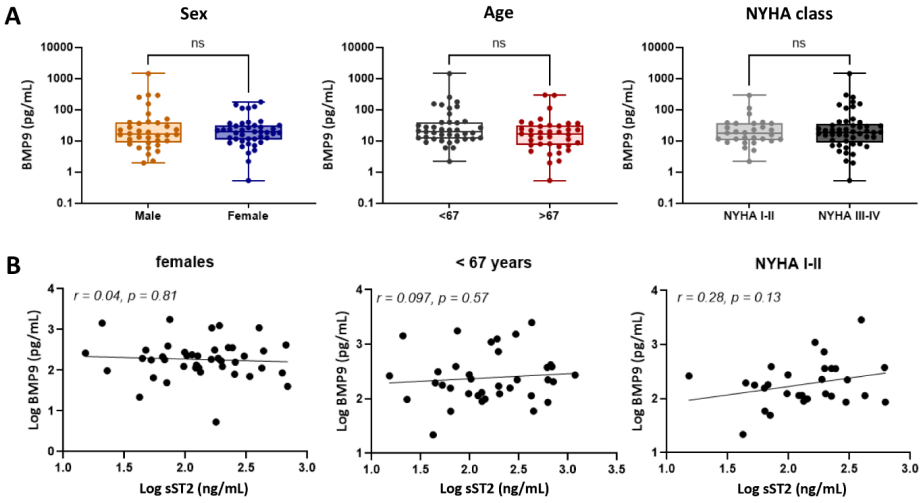

Figure S5. No positive correlation between sST2 and BMP9 levels in stratified PAH Groups. (A) Circulating levels of BMP9 in PAH patients stratified by sex, age, and NYHA class (N=79). (B) Correlation between circulating sST2 and BMP9 in sub-stratified groups with low circulating sST2 levels.